

## DISTANCES AND KINEMATICS OF GOULD BELT STAR-FORMING REGIONS WITH GAIA DR2 RESULTS

SERGIO A. DZIB,<sup>1</sup> LAURENT LOINARD,<sup>2,3</sup> GISELA N. ORTIZ-LEÓN,<sup>1,4</sup> LUIS F. RODRÍGUEZ,<sup>2</sup> AND PHILLIP A. B. GALLI<sup>5</sup>

<sup>1</sup>*Max-Planck-Institut für Radioastronomie, Auf dem Hügel 69, D-53121 Bonn, Germany*

<sup>2</sup>*Instituto de Radioastronomía y Astrofísica, Universidad Nacional Autónoma de México, Morelia 58089, Mexico*

<sup>3</sup>*Instituto de Astronomía, Universidad Nacional Autónoma de México, Apartado Postal 70-264, CdMx C.P. 04510, Mexico*

<sup>4</sup>*Humboldt Fellow*

<sup>5</sup>*Laboratoire d'astrophysique de Bordeaux, Univ. Bordeaux, CNRS, B18N, allée Geoffroy Saint-Hillaire, 33615 Pessac, France.*

### ABSTRACT

We present an analysis of the astrometric results from Gaia second data release (DR2) to Young Stellar Objects (YSOs) in star-forming regions related to the Gould Belt. These regions are Barnard 59, Lupus 1 to 4, Chamaeleon I and II,  $\epsilon$ -Chamaeleontis, the Cepheus flare, IC 5146 and Corona Australis. The mean distance to the YSOs in each region are consistent with earlier estimations, though a significant improvement to the final errors was obtained. The mean distances to the star-forming regions were used to fit an ellipsoid of size  $(358 \pm 7) \times (316 \pm 13) \times (70 \pm 4)$  pc, and centered at  $(X_0, Y_0, Z_0) = (-82 \pm 15, 39 \pm 7, -25 \pm 4)$  pc, consistent with recently determined parameter of the Gould Belt. The mean proper motions were combined with radial velocities from the literature to obtain the three dimensional motion of the star-forming regions, which are consistent with a general expansion of the Gould Belt. We estimate that this expansion is occurring at a velocity of  $2.5 \pm 0.1$  km s<sup>-1</sup>. This is the first time that YSOs motions are used to investigate the kinematic of the Gould Belt. As an interesting side result, we also identified stars with large peculiar velocities.

*Keywords:* astrometry — stars:formation — stars:kinematics

arXiv:1810.01917v1 [astro-ph.SR] 3 Oct 2018

## 1. INTRODUCTION

In the 19<sup>th</sup> century, Sir John Herschel and, a few decades later, Professor Benjamin Gould noticed that the brightest stars in the sky defined a partial ring that crossed the Milky Way with an inclination angle of  $\sim 20^\circ$ . Nowadays, we know that this structure is composed of gas and young stars and, in fact, most of the nearby star-forming regions are part of this structure, now called the Gould Belt (GB). The classical assumed structure for the GB is an elliptical ring traced mainly by clouds and OB stars. However analysis of X-ray active stars have shown that a filled disk structure may be more appropriate (Guillout et al. 1998). The origin of the GB is still uncertain, but there are suggestions that its origin is due to the collision of a high-velocity cloud (or dark matter dominated clump) with the Galactic plane (Comeron 1993; Bekki 2009).

The GB semi-major axes are between 200 and 400 pc and its center lies around 100 pc away from the Sun in the direction of the Galactic anti-center (e.g., Perrot & Grenier 2003). Then, even when some star forming regions lie in projection to the so-called GB-plane their heliocentric distances,  $> 500$  pc, do not match with the main structure, and are not considered part of the GB<sup>1</sup>. On the other hand, there are star forming regions in the solar neighborhood whose positions are projected in directions far apart from the GB-plane (e.g., Chamaeleon clouds and Corona Australis) making their membership in the GB debatable. These deviations may simply reflect the thickness of the GB disk.

Distances to GB star-forming regions have been controversial and historically have been affected by uncertainties of around 30% (e.g. see next subsection). In recent years, Very Long Baseline Interferometry (VLBI) has helped to estimate the distance with a few percents of accuracy to Young Stellar Objects (YSOs) with strong magnetic activity that produces non-thermal radio emission (e.g., Ortiz-León et al. 2017a,b; Kounkel et al. 2017; Dzib et al. 2018; Galli et al. 2018, and references therein). In all cases, these estimations allowed to obtain a mean distance, the depth, and the kinematics of the regions where they belong.

A major milestone in modern astrometry is the Gaia space mission (Gaia Collaboration et al. 2016). Gaia has measured the positions ( $\alpha$ ,  $\delta$ ), proper motions ( $\mu_\alpha$ ,  $\mu_\delta$ ), and parallaxes ( $\pi$ ) of billions of stars in its second data release (Gaia Collaboration et al. 2018). The dust obscures the optical emission of many of the YSOs in star-forming regions so that they cannot be detected by the Gaia satellite. However, Gaia does provide the distance to YSOs that are not highly embedded

and to the brightest members, making it possible to determine the distance and kinematics to these star-forming regions.

### 1.1. Star-forming regions in Gould Belt

Around a dozen star-forming regions have been associated with the GB. Our analysis is focused on the regions whose distance, position, or kinematic would suggest an association with the GB (Perrot & Grenier 2003; Ward-Thompson et al. 2007). We introduce these regions below. Other star-forming regions will be discussed in parallel papers: Perseus by Ortiz-León et al. (2018), Ophiuchus and Serpens by Ortiz-León et al. (in prep.), and Taurus by Galli et al. (in prep.).

*Barnard 59* (B59) is the only cloud in the Pipe Nebula complex with star formation activity (Alves et al. 2008). There are around 20 embedded YSOs in the B59 cloud (Brooke et al. 2007) which will be used as our target sample for this region. Earlier studies suggested a distance of 160 pc (Reipurth & Zinnecker 1993). However, recent studies performed by Lombardi et al. (2006) and Alves & Franco (2007) yield distances of  $130^{+24}_{-58}$  pc and  $145 \pm 16$  pc, respectively. These authors used Hipparcos data of field stars. Recently, Dzib et al. (2016) obtained radio observations to search for YSOs with non-thermal radio emission to later observe them with the VLBI technique and determine a distance, however, even when nine stars were detected in the radio no clear candidates to observe with VLBI were found. Thus, a direct estimation of the distance to this region is necessary.

The *Cepheus Flare* is a coherent giant molecular cloud complex (size  $\sim 100$  pc; Olano et al. 2006) with dense gas distributed in a wide range of radial velocities (from  $-15$  to  $15$  km  $s^{-1}$ ; Hu 1981; Lebrun 1986; Kun et al. 2008). The wide range of motion of the gas may reflect multiple supernova events in the past. These supernovas may have also sustained the star formation in this region (Kun et al. 2008). Distance determinations to the different components of the complex agree with the conclusion that these are distributed between 300 pc and 500 pc (Kun et al. 2008, and references therein). Kun et al. (2008) compiled a list of YSOs in the Cepheus region that we will use as input for our analysis. Towards the Cepheus flare region, there are other more distant star-forming regions, of which the most active is NGC 7129. Many of the pre-main sequence stars found in the Cepheus flare are part of this region (Kun et al. 2008). NGC 7129, however, seems to be at a larger distance of 1 kpc (Racine 1968; Straižys et al. 2014).

*Chamaeleon* is divided into three different main clouds, each in a different evolutionary stage. While Chamaeleon I (Cha I) is actively forming stars, Chamaeleon III (Cha III) has no evidence of star formation; and Chamaeleon II (Cha II) is in an intermediate phase of forming stars. The input list of YSOs was taken mainly from the stars listed in Luhman

<sup>1</sup> For example, the Monoceros R2 region lies in the direction of the Orion Nebula Cluster, a star forming region that belongs to the GB, it is however at a distance of 900 pc (Dzib et al. 2016), thus far away from the GB.

(2008, see also the references therein) for the two star forming regions in Chamaeleon. Luhman (2008) discussed the distances measured in the last few decades. For Cha I, photometric works point to distances between 135 pc and 165 pc, while the Hipparcos parallax to star members are more consistent with a distance around 175 pc. On the other hand, the extinction measurements towards Cha II point to a distance of  $178 \pm 18$  pc. Recently, Voirin et al. (2018) using data from Gaia DR1, estimated distances of  $179_{-10,-10}^{+11,+11}$  pc,  $181_{-5,-10}^{+6,+11}$  pc, and  $199_{-7,-11}^{+8,+12}$  pc, for Cha I, Cha II, and Cha III, respectively. In the area between these clouds, there is a nearby ( $d \sim 114$  pc) and relatively old ( $\tau \sim 6$  Myr) group of YSOs, known as the  $\epsilon$  Chamaeleontis ( $\epsilon$  Cha) group (Feigelson et al. 2003; Luhman 2004).

*Corona Australis* (CrA) is one of the nearest clouds with ongoing low- and intermediate-mass star formation with most of its YSO population in the Coronet protostar cluster (see Neuhäuser & Forbrich 2008, for a review of this region). In their review Neuhäuser & Forbrich (2008) compile the young stellar members on this region, which we use as the input list. Distance estimates toward CrA vary from 120 to 170 pc, with the best estimation being around 130 pc (Neuhäuser & Forbrich 2008). It was discarded as part of the GB by Olano (1982) since it is located at a Galactic latitude too low compared to that of the GB plane. However, it has been suggested that the 3D motion of its T Tauri stars is consistent with the cloud being formed by the impact of a high-velocity cloud onto the Galactic plane, and thus consistent with the formation of the GB. Nevertheless, alternative scenarios cannot be ruled out (Neuhäuser et al. 2000).

IC 5146 is a nebula that is in the transition between a reflection nebula and an HII region (Herbig & Reipurth 2008). It has been associated with a large population of YSOs, whose most massive member, the B0 V star BD+46°3474, illuminates and ionizes the gas. The population of YSOs was listed by Herbig & Reipurth (2008) in their review of this region. The distance to IC 5146 is still quite uncertain. Early works suggested a distance around 1 kpc (Elias 1978; Crampton & Fisher 1974), but later Lada et al. (1999) suggested a shorter distance of 460 pc, based on counts of foreground stars. More recently, different works suggest that the distance to this massive star-forming region is between 900 and 1400 pc (see discussion by Herbig & Reipurth 2008, and references therein). The position of IC 5146 on the plane of the sky is consistent with the GB-plane, thus its membership in the GB strongly depends on an accurate measurement of its distance.

The *Lupus* complex is formed of nine clouds (named as Lupus 1 to 9) and it has been recognized as one of the main low-mass star-forming region within 200 pc of the Sun (Comerón 2008). Most of the star-forming activity is concentrated in Lupus 3, and it has the densest population of YSOs in the complex. Other clouds that are forming stars are Lu-

pus 1, 2, and 4. Lupus 4 contains  $\text{H}^{13}\text{CO}^+$  cores that are signs of future star formation (Comerón 2008). The other clouds have no star formation activity. The input list of YSOs for this complex was taken from the work by Comerón (2008), who compiled the YSO population at the different evolutionary stages. In his review of this complex, Comerón (2008) argued that a single distance to the whole complex seems inadequate, and suggested values of 200 pc for Lupus 3, and 150 pc for the rest of the clouds. More recently, kinematic studies performed by Galli et al. (2013) show that the distances to Lupus 1 and Lupus 3 are  $182_{-6}^{+7}$  and  $185_{-10}^{+11}$  pc, respectively, i.e., they are consistent with each other within their errors bars.

## 2. DATA AND METHODS

We compiled an initial list of known young stars in the regions mentioned above from the literature and we complemented with sources from the Simbad database. Then we searched in the Gaia archive database which stars from this list have an astrometric solution for the five parameters ( $\alpha$ ,  $\delta$ ,  $\mu_{\alpha,*} = \mu_{\alpha} \cos \delta$ ,  $\mu_{\delta}$ , and  $\pi$ ). The maximum allowed separation between the position in the literature of the YSOs and the objects in the Gaia catalog was  $1''$ . We also discarded those YSOs whose trigonometric parallax is negative or indicative of a distance well beyond the value estimated for the regions where they belong. These odd results indicate that their Gaia solution needs to be revisited or that the stars in question actually do not belong to the region. The YSOs used for the analysis in the following sections are listed in Table 1.

To obtain a mean parallax and the dispersion measure to the individual regions, a histogram of the parallaxes was constructed for each region. Then these histograms were fitted with a Gaussian distribution model. To obtain the distance to the regions we apply the well known relation  $d[\text{pc}] = 1/\pi['']$ . In a similar fashion, and following Dzib et al. (2017), we also constructed histograms of the proper motions and fitted Gaussian distribution models to them. This procedure is also used to recognize stars moving with peculiar proper motions (i.e., stars with  $|\mu - \bar{\mu}| > 3\sigma_{\mu}$ , where  $\bar{\mu}$  is the mean proper motion of each cloud, see also Dzib et al. 2017). In the regions where only few YSOs are in the Gaia DR2 catalog, we obtain the main values in parallax and proper motions by averaging the individual values.

## 3. RESULTS AND DISCUSSION OF INDIVIDUAL REGIONS

Using the methods described in the previous section, we determined the mean trigonometric parallax to the star-forming regions introduced in Section 1. The mean trigonometric parallaxes and the corresponding distances are presented in Table 2. The trigonometric parallax dispersion ( $\sigma_{\pi}$ ) is dominated by the errors of the individual parallaxes

**Table 1.** Astrometric parameters of YSOs used in our analysis from the Gaia-DR2 catalog (Gaia Collaboration et al. 2018).

YSO Name	R.A. (°)	Dec. (°)	$\pi$ (mas)	$\mu_{\alpha_*}$ (mas yr <sup>-1</sup> )	$\mu_{\delta}$ (mas yr <sup>-1</sup> )	Region
EM* LkHA 346	257.8220029	-27.4190194	7.21 ± 1.11	-5.54 ± 2.38	-10.88 ± 1.76	Barnard 59
2MASS J17113036-2726292	257.8765466	-27.4415534	6.39 ± 0.19	2.37 ± 0.34	-19.94 ± 0.23	Barnard 59
2MASS J17112701-2723485	257.8625319	-27.3969175	6.02 ± 0.53	-0.50 ± 1.13	-16.58 ± 0.78	Barnard 59
2MASS J17112942-2725367	257.8725897	-27.4270103	6.18 ± 0.63	-0.83 ± 1.17	-19.01 ± 0.84	Barnard 59
2MASS J17112729-2725283	257.8637175	-27.4246713	7.10 ± 0.70	1.21 ± 1.40	-18.33 ± 0.95	Barnard 59
2MASS J17114182-2725477	257.9243060	-27.4299610	6.35 ± 0.06	-0.91 ± 0.10	-17.91 ± 0.07	Barnard 59
2MASS J17111182-2726547	257.7992678	-27.4486738	6.20 ± 0.54	-1.23 ± 1.08	-18.92 ± 0.76	Barnard 59
2MASS J17111445-2726543	257.8102231	-27.4485307	6.26 ± 0.21	-0.10 ± 0.40	-19.05 ± 0.26	Barnard 59
[BHB2007] 18NE	257.9238374	-27.4307035	6.18 ± 0.09	-0.50 ± 0.15	-18.20 ± 0.10	Barnard 59
2MASS J17110411-2722593	257.7671511	-27.3832858	5.92 ± 0.30	-1.41 ± 0.59	-21.63 ± 0.34	Barnard 59

NOTE—Table 1 is published in its entirety in the machine-readable format. A portion is shown here for guidance regarding its form and content.

**Table 2.** Studied star forming regions in the Gould Belt and their position in Galactic coordinates. The number of YSOs used in the studied regions and the mean and dispersion measurement of trigonometric parallaxes to each region are presented. The median of individual trigonometrical parallax errors is also presented for comparison with the dispersion measurement. The corresponding distances and final errors to each region are also listed.

Region	$l$ (°)	$b$ (°)	# YSOs	$\bar{\pi} \pm \varepsilon_{\bar{\pi}}$ (mas)	$\sigma_{\pi}$ (mas)	$\varepsilon_{\bar{\pi}}$ (mas)	$\bar{D}$ (pc)	$\varepsilon_{\bar{D}}$ (pc)
Barnard 59	357.0	+07.1	11	6.12 ± 0.03	0.16	0.40	163	5
Cepheus Flare	110.0	+15.0	47	2.79 ± 0.04	0.22	0.10	358	32
Cepheus - NGC 7129	105.4	+09.9	40	1.08 ± 0.04	0.16	0.12	926	163
Chamaeleon I	297.2	-15.4	71	5.21 ± 0.01	0.13	0.09	192	6
Chamaeleon II	303.6	-14.4	12	5.05 ± 0.02	0.09	0.07	198	6
$\epsilon$ Chamaeleontis	300.3	-14.0	19	9.93 ± 0.03	0.11	0.05	101	2
Corona Australis	359.9	-17.8	21	6.48 ± 0.02	0.13	0.09	154	4
IC 5146	094.4	-05.5	62	1.23 ± 0.03	0.12	0.12	813	106
Lupus 1	338.8	+15.7	9	6.41 ± 0.01	0.06	0.06	156	3
Lupus 2	338.9	+12.1	4	6.31 ± 0.01	...	0.06	159	3
Lupus 3	339.6	+09.4	49	6.16 ± 0.01	0.13	0.08	162	3
Lupus 4	336.3	+08.2	11	6.13 ± 0.02	0.10	0.13	163	4

( $\varepsilon_{\bar{\pi}}$ ), since the median of these errors is similar to the parallax dispersion (see Table 2), thus they represent an uncertainty in the mean distance to the region rather than a sign of their depth. Our final error, then, will be obtained by adding in quadrature the error of the mean trigonometric parallax ( $\varepsilon_{\bar{\pi}}$ ), the parallax dispersion ( $\sigma_{\pi}$ ) and the systematic errors of 0.1 mas of the Gaia DR2 results (Luri et al. 2018), being the last two the dominant sources of errors. The estimated distances to the star-forming regions are in good agreement with

previous estimations but we found a significant improvement on the final errors.

The proper motion measured by the Gaia mission contain the reflex solar motion. This motion is, in some cases, the dominant contribution to the proper motion vector. We have calculated the resulting proper motions by using a Solar motion of ( $U_{\odot}, V_{\odot}, W_{\odot}$ ) = (11.1 ± 0.7, 12.2 ± 0.47, 7.25 ± 0.37) km s<sup>-1</sup> (Schönrich et al. 2010) and the Galacto-centric distance of 8.4 kpc (Reid et al. 2009). The values for each

**Table 3.** List of mean proper motions of the studied regions and the corresponding linear velocities. The proper motion and velocity dispersions are also listed. The reflex solar proper motions are also listed.

Region	$\mu_{\odot}$		$\mu$		Velocity <sub>sky</sub>		$\sigma_{\mu}$		$\sigma_{\text{Vel.}}$	
	$\alpha_*$	$\delta$	$\alpha_*$	$\delta$	$\alpha_*$	$\delta$	$\alpha_*$	$\delta$	$\alpha_*$	$\delta$
	(mas yr <sup>-1</sup> )		(mas yr <sup>-1</sup> )		(km s <sup>-1</sup> )		(mas yr <sup>-1</sup> )		(km s <sup>-1</sup> )	
Barnard 59	-3.5	-17.9	-1.2 ± 0.2	-19.2 ± 0.1	-0.9 ± 0.2	-14.9 ± 0.1	0.23	0.37	0.2	0.3
Cepheus Flare	8.3	3.7	5.8 ± 0.3	0.4 ± 0.7	9.9 ± 0.5	0.7 ± 1.2	1.7	3.1	2.8	5.3
Cepheus - NGC 7129	3.2	1.1	-1.89 ± 0.02	-3.51 ± 0.05	-7.8 ± 0.1	-14.6 ± 0.2	0.26	0.43	1.1	1.8
Chamaeleon I	-18.0	1.3	-22.8 ± 0.1	0.3 ± 0.1	-20.6 ± 0.1	0.3 ± 0.1	0.90	1.25	0.8	1.1
Chamaeleon II	-16.7	-7.2	-20.7 ± 0.1	-7.8 ± 0.1	-19.1 ± 0.1	-7.3 ± 0.1	0.72	0.42	0.7	0.4
ε Chamaeleontis	-16.7	-7.2	-40.3 ± 0.2	-7.3 ± 0.7	-19.2 ± 0.1	-3.5 ± 0.3	1.24	1.60	0.5	1.1
Corona Australis	7.2	-20.7	4.4 ± 0.2	-27.3 ± 0.2	3.2 ± 0.2	-19.8 ± 0.2	1.46	1.09	1.1	0.8
IC 5146	3.8	0.3	-2.96 ± 0.01	-2.96 ± 0.03	-11.0 ± 0.04	-11.0 ± 0.1	0.39	0.41	1.5	1.5
Lupus 1	-11.5	-18.9	-15.0 ± 0.1	-23.3 ± 0.1	-11.1 ± 0.1	-17.7 ± 0.1	0.74	0.67	0.6	0.5
Lupus 2	-10.3	-19.3	-10.7 ± 0.1	-22.0 ± 0.1	-8.0 ± 0.1	-16.5 ± 0.1	...	...	...	...
Lupus 3	-9.1	-19.5	-10.0 ± 0.1	-23.7 ± 0.1	-7.5 ± 0.1	-17.9 ± 0.1	0.78	0.63	0.6	0.5
Lupus 4	-8.1	-19.4	-11.9 ± 0.2	-23.9 ± 0.2	-9.2 ± 0.2	-18.5 ± 0.2	1.0	0.5	0.8	0.4

region are listed in Table 3 to compare them with their estimated mean values.

The estimated global proper motions to each star-forming region are shown in Table 3 together with the proper motion dispersions. Tangential velocities and velocity dispersions were calculated according to the mean distance to each region and are also presented in Table 3. In the following, we will describe the individual results for each region.

### 3.1. Barnard 59

From the 22 YSOs and YSO candidates in this region, we find that 11 are in the Gaia DR2 catalog. The mean trigonometric parallax of  $6.12 \pm 0.19$  mas to the stars corresponds to a distance of  $163 \pm 5$  pc for this region (see Table 2 and top panels of Figure 1). All the stars agree within errors with this value, even the two with the larger trigonometric parallaxes of  $7.2 \pm 1.1$  mas, and  $7.1 \pm 0.7$  mas.

The mean distance to B59 seems to be larger than the earlier estimations, but they agree within the errors. As the mean distance obtained by us is based on known YSOs in the region, we are more confident with it. This new distance also shows an improvement in the accuracy, that is now 3%.

The proper motion of one of the stars, named [BHB2007] 7 or LkH $\alpha$  346 (Brooke et al. 2007), indicates that it is also moving differently than the remaining YSOs, as it can be seen in the bottom panels of Figure 1. The proper motion of this star differs by about  $10 \text{ mas yr}^{-1}$  from the mean of the rest of the stars. This difference corresponds to about  $8 \text{ km s}^{-1}$  at a distance of 163 pc. This suggests that LkH $\alpha$  346 may be escaping from the region.

### 3.2. Cepheus Flare

Despite being widely spread on the plane of the sky, the YSOs in the Cepheus flare show a good agreement between parallax measurements and give a mean value of  $2.78 \pm 0.25$  mas (see top panels of Figure 2). The corresponding distance is  $360 \pm 32$  pc. This value is in the range of the distances, 300 to 500 pc, estimated for this complex based on previous determinations on the literature (see Kun et al. 2008, and references therein). In the top-right panel of Figure 2, we show the spatial distribution of these YSOs colored by their corresponding distances. From this image, we can see that the YSOs to the north of the complex seem to be farther than those in the south.

The proper motion dispersions are large compared to the other regions (see Table 3 and Figure 2). This could reflect the fact that the YSOs were formed in different clouds within the complex, and thus with slightly different kinematics.

There are only three stars that are moving well beyond the mean proper motion of the other stars, especially in the R.A. direction. These stars are [KBK2009b] 119, 2MASS J21440537+6605531, and BD+65°1636. The last two objects are projected in the direction of NGC 7129 (see next section). However, their determined trigonometric parallaxes ( $3.3 \pm 0.4$  mas and  $3.09 \pm 0.04$  mas for 2MASS J21440537+6605531 and BD+65°1636, respectively) show that they are at a much shorter distance and do not belong to NGC 7129.

### 3.3. Cepheus - NGC 7129

Almost half of the YSO population in the Cepheus flare with astrometric results in the Gaia DR2 catalog are concen-

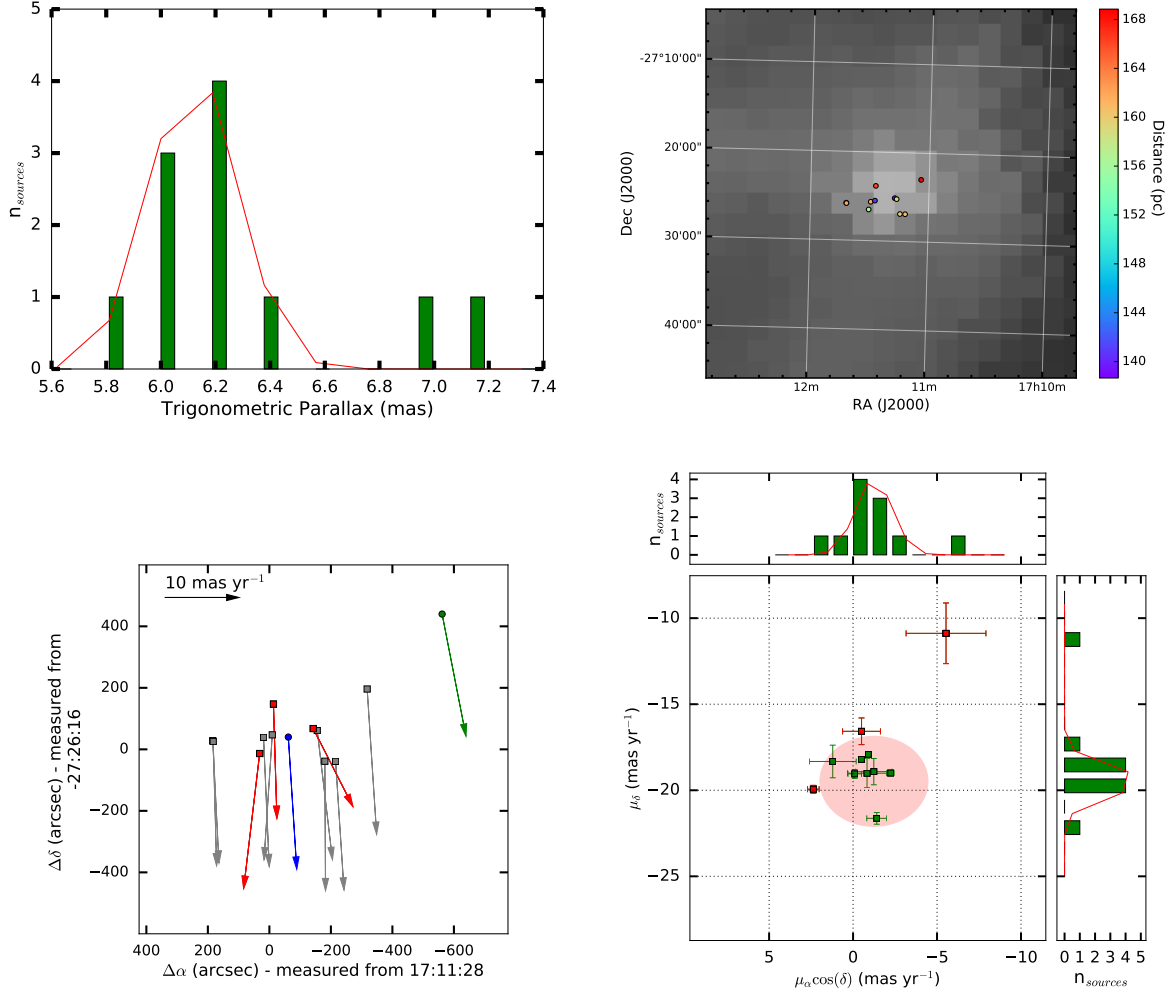


**Figure 1.** *Top-left:* Histogram of individual trigonometric parallaxes to YSOs in the B59 region. The red line is the Gaussian fit to the histogram. *Top-right:* Distribution of YSOs in the B59 region, colored by their corresponding distance from Gaia DR2 trigonometric parallaxes. *Bottom-left:* Proper motion vectors of YSOs in B59. In grey arrows we plot those proper motions that are within three times the dispersion, while the red arrows are the outliers of the proper motion distribution. The blue arrow indicates the vector of the mean proper motion of the stars in the B59 region (as given in Table 2). The green arrow indicate the reflex proper motion as due to the Solar motion at the Galactic position of B59. *Bottom-right:* Proper motion distribution of YSOs in B59. Red circle represents three times the dispersion measurement constrain to identify YSOs with peculiar motions. Histograms and gaussian fits (red lines) of the proper motions in R.A. (top) and Dec. (right), are also shown.

trated in the NGC 7129 region. The mean trigonometric parallax of the region of  $1.08 \pm 0.19$  mas confirms that the distance to this region,  $926 \pm 163$  pc (see top panels of Figure 3), is larger than that of the Cepheus flare located at  $360 \pm 32$  pc. Thus, it does not belong to this complex.

The proper motions of the stars in NGC 7129 are well concentrated around  $\mu_\alpha = -1.89 \pm 0.02$  mas yr<sup>-1</sup>, and  $\mu_\delta = -3.51 \pm 0.05$  mas yr<sup>-1</sup>. As can be seen in the bottom panels of Figure 3, four cases are outside the  $\pm 3\sigma_\mu$  from the mean and one is consistent with within errors. These objects are 2MASS J21424705+6604578, 2MASS J21424687+6606574, 2MASS J21431161+6609114, and 2MASS J21430502+6606533. In compact clusters such as NGC 7129, fast moving stars may be produced by  $n$ -body interactions (Poveda et al. 1967), as has been observed in

Orion (e.g., Dzib et al. 2017). In NGC 7129 this may be the case as well.

### 3.4. *Chamaeleon*

Most of the star formation in the Chamaeleon complex is occurring in the Cha I cloud, and we found that 71 of the YSOs in this cloud are in the Gaia DR2 catalog. We also found 13 YSOs in Cha II and 19 dispersed YSOs that belong to  $\epsilon$  Cha. The trigonometric parallaxes and proper motions of the YSOs of each individual region have low dispersion (see Tables 2 and 3 and Figures 4, 5, and 6), as expected if they are part of the same group of stars.

Our results also show that the two main clouds of the complex are at similar distances as it has been found previously. These distances agree within errors with those recently found

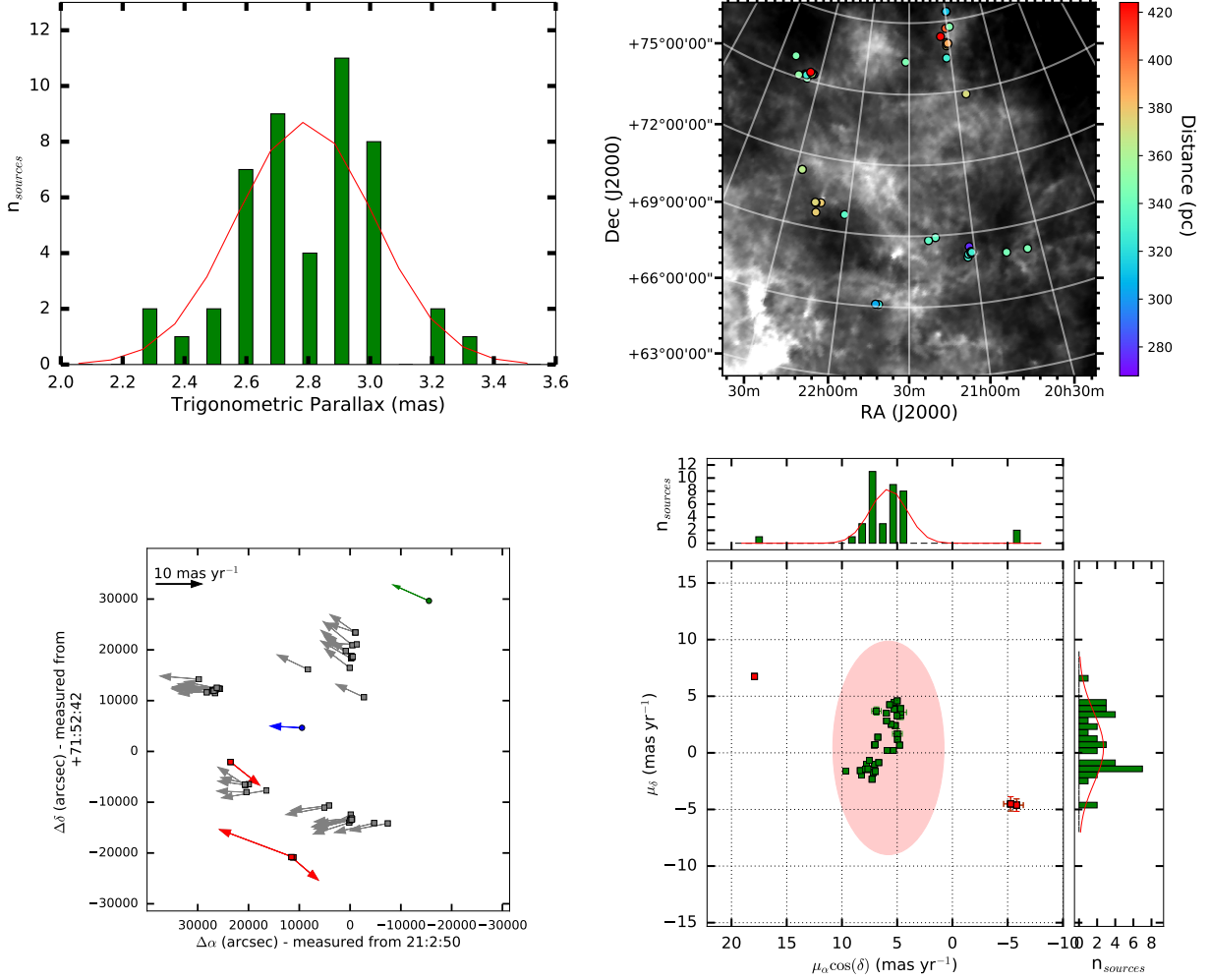


**Figure 2.** Same as Figure 1, but for the Cepheus flare region.

by [Voirin et al. \(2018\)](#), but their errors are slightly larger. The distance to the group  $\epsilon$  Cha is shorter than earlier estimations (i.e., 114 pc; [Feigelson et al. 2003](#)).

The mean proper motions of Cha I and Cha II show that they are moving in slightly different directions. The mean proper motions in right ascension are similar for objects in both clouds, but not in the declination direction. Also, while all the proper motions of YSOs in the Cha II are inside the  $3\sigma_\mu$  from the mean, in Cha I three objects show peculiar motions: [CCE98] 1-74, Ass Cha T 1-23, and V\* CS Cha. Their peculiar motion may be originated from interaction with other YSOs in the cloud. In  $\epsilon$  Cha, on the other hand, the proper motion dispersion is larger, as expected for a more dispersed population. To take this into account for the identification of objects with peculiar motions we relaxed our constrain from  $3\sigma_\mu$  to  $5\sigma_\mu$ . Only the YSO RX J1123.2-7924 has a large peculiar motion. The Gaia DR2 proper motions of this object are  $\mu_\alpha = -31.7 \pm 0.1$  mas yr $^{-1}$  and  $\mu_\delta = -17.4 \pm 0.1$  mas yr $^{-1}$ , which corresponds to a relative proper motion with respect to the group of  $\Delta\mu = 13.3 \pm 0.7$  mas yr $^{-1}$ .

At a distance of 100.7 pc, the star is moving at a velocity of  $6.4 \pm 0.3$  km s $^{-1}$ . In conclusion, even when the star has a high peculiar motion with respect to the rest of the group it is not a fast-moving source.

### 3.5. Corona Australis

The mean trigonometric parallax of CrA suggests a distance of  $154 \pm 4$  pc, which is significantly larger than that presented by [Neuhäuser & Forbrich \(2008\)](#), and references therein). The mean proper motions are in good agreement with the values of  $(\mu_\alpha \cdot \cos \delta, \mu_\delta) \simeq (5.5, -27.0)$  mas yr $^{-1}$  estimated by [Neuhäuser et al. \(2000\)](#) based on results of different catalogs.

One of the stars in the CrA region is above the  $3\sigma_\mu$  criteria, it is named [MR81] H $\alpha$  17. The peculiar proper motion of this star is  $5.4 \pm 0.4$  mas yr $^{-1}$  and corresponds to peculiar velocity of  $4.0 \pm 0.3$  km s $^{-1}$ .

### 3.6. IC 5146

Our results show that the mean trigonometric parallax of YSOs in IC 5146 agrees with a distance of  $813 \pm 106$  pc. This

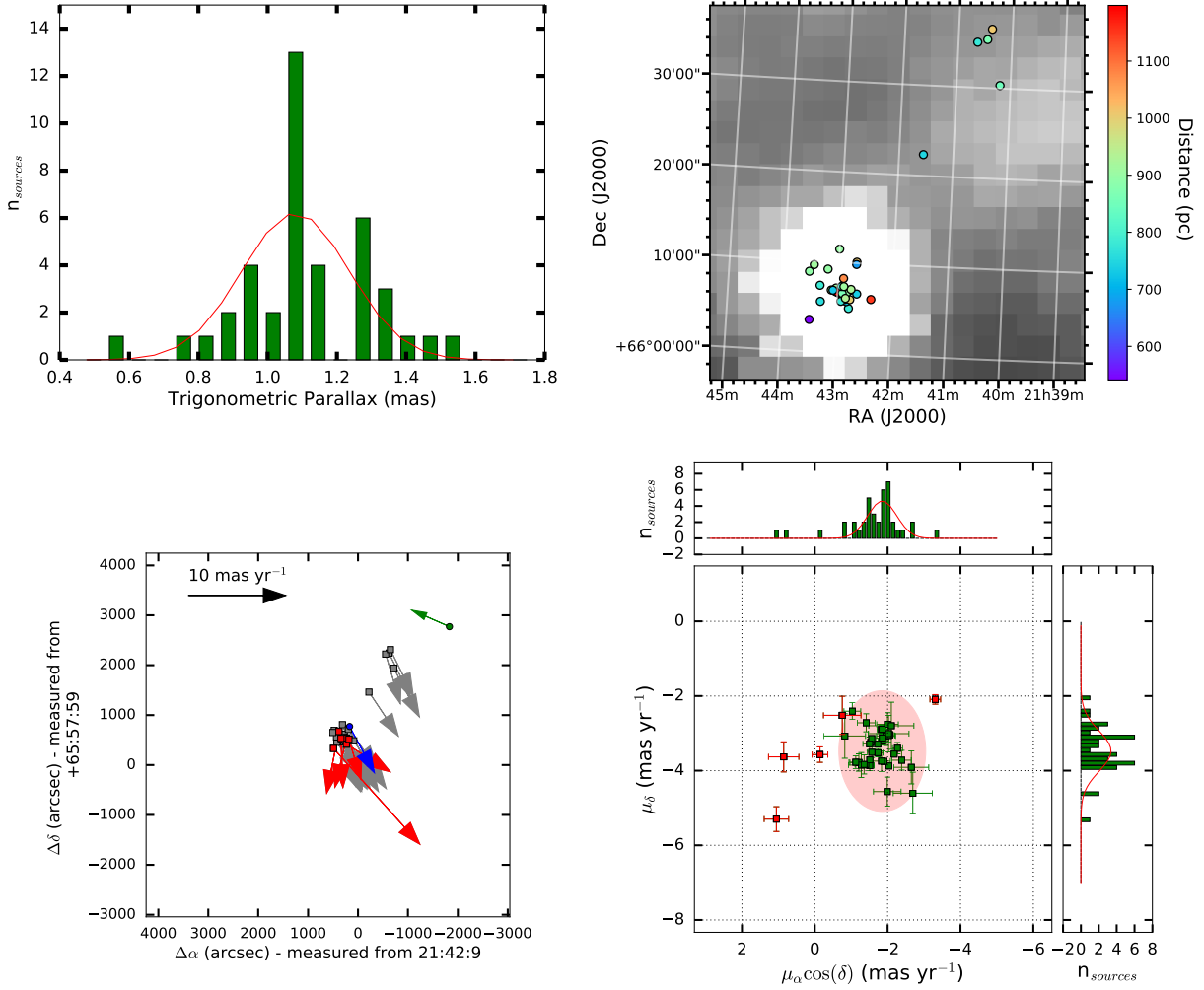


**Figure 3.** Same as Figure 1, but for the Cepheus - NGC 7129 region.

value is consistent with the more recent values found in this nebula and discards the short distance of 460 pc obtained by Lada et al. (1999) and Lada et al. (1994). Thus, this region is not part of the Gould Belt.

Five of the stars in IC 5146 have proper motions that do not agree, within errors, with our  $3\sigma_\mu$  criteria. Two of these stars, LkH $\alpha$  255 and LkH $\alpha$  241, have the largest peculiar motions and are at the edges of the cloud (see Figure 8). The proper motions of LkH $\alpha$  241 are  $(\mu_\alpha \cdot \cos \delta, \mu_\delta) \simeq (4.1 \pm 0.3, -8.5 \pm 0.2)$  mas yr $^{-1}$ , indicating a relative proper motion with respect to the main group of  $9.4 \pm 0.4$  mas yr $^{-1} \simeq 36.3 \pm 1.5$  km s $^{-1}$ , with a direction towards the cluster. The motion of LkH $\alpha$  255 points away from the cluster. Its proper motions are  $(\mu_\alpha \cdot \cos \delta, \mu_\delta) \simeq (-6.9 \pm 0.4, 1.1 \pm 0.4)$  mas yr $^{-1}$ , or a relative motion of  $5.6 \pm 0.4$  mas yr $^{-1} \simeq 21.3 \pm 2.3$  km s $^{-1}$ . The velocities of these two stars indicate that they are fast moving stars.

### 3.7. Lupus

Contrary to what was suggested by Comerón (2008) the distances to the YSOs in the Lupus clouds indicate that they all are at a distance around 160 pc. This distance is also significantly shorter than the kinematic distance found by Galli et al. (2013), and in agreement with the earlier determination of the distance to this region (e.g., Franco 1990; Crawford 2000; Lombardi et al. 2008).

The mean proper motions of the four clouds seem to be also similar. Only the Lupus 1 cloud has a slightly different mean proper motion in the R.A. direction. This may indicate that even when the four regions are well constrained, the clouds where they form were not independent and probably were part of a large cloud.

As in the other regions, we also identified YSOs with peculiar motions in the Lupus clouds. The star with the most peculiar velocity in this region is the YSO THA 15 36. It has proper motions of  $(\mu_\alpha \cdot \cos \delta, \mu_\delta) \simeq (-17.5 \pm 0.1, -26.4 \pm 0.1)$  mas yr $^{-1}$ . This motion will imply a relative motion of  $8.0 \pm 0.2$  mas yr $^{-1} \simeq 6.1 \pm 0.2$  km s $^{-1}$  with respect to the



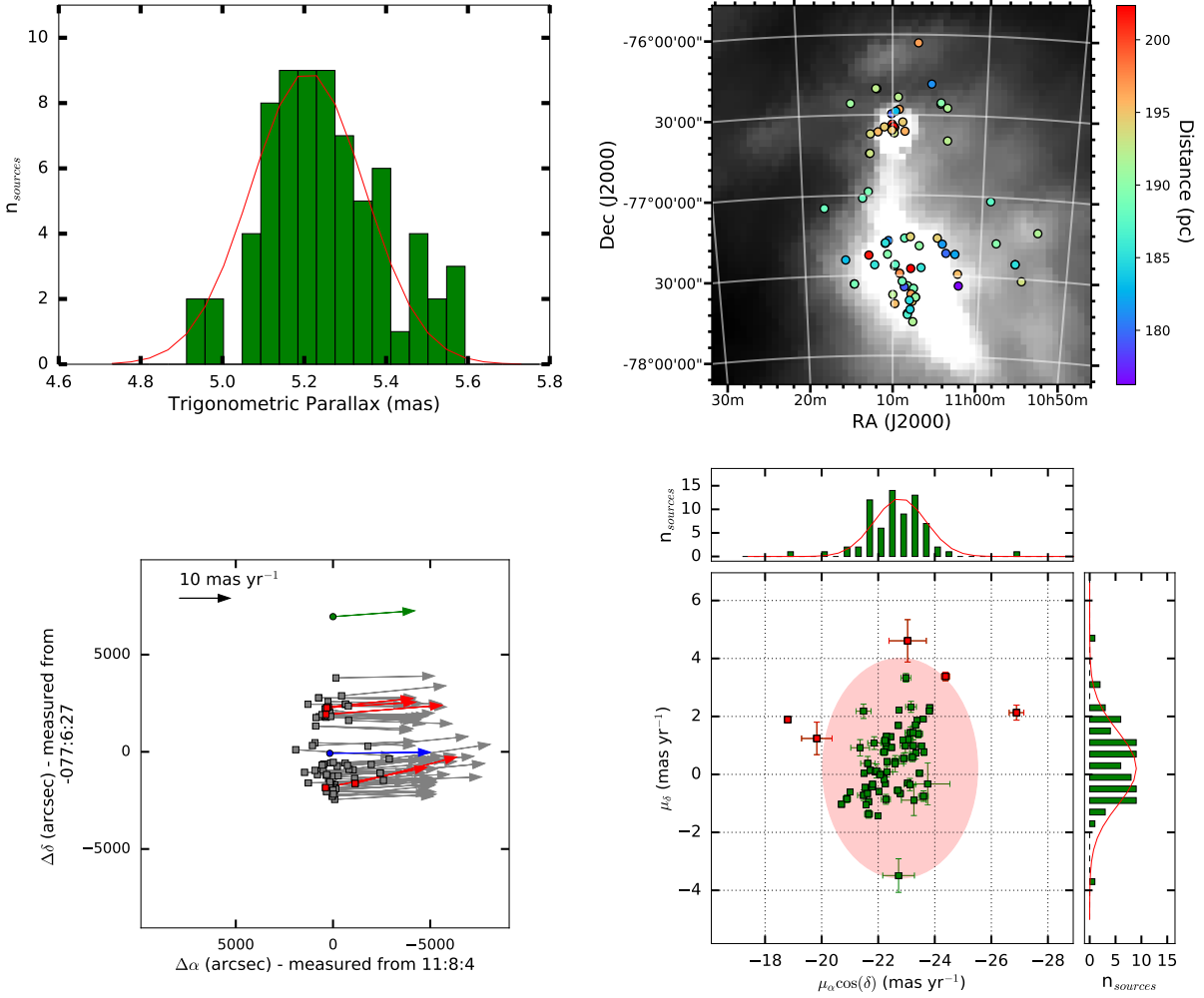


**Figure 4.** Same as Figure 1, but for Chamaeleon I.

other YSOs. The velocity of this star indicates that it is not a fast moving object. As the same analysis may be applied to the other object, we conclude that none of the YSOs that we analyzed in the Lupus clouds are fast moving sources.

#### 4. GOULD BELT KINEMATICS

In order to re-construct the three dimensional kinematics of star-forming regions in the Gould Belt, we will use the mean proper motions of the YSOs of regions listed in Tab. 3 with distances  $120 < d[\text{pc}] < 500$ . Additionally to them, we will also use other star-forming regions whose distances and mean proper motions have been studied in other papers and are also suggested to belong to the GB. These regions are: the Orion Nebula Cluster (ONC), L1688 in Ophiuchus, IC 348 and NGC 1333 in Perseus, and L 1495 in Taurus. The clouds in the Taurus complex are known to lie near the GB center, which is inconsistent with the classical picture of the ring structure, however, since we are also considering the possibility of a filled disk, they will be used for the following analysis. All the regions used for this new analysis are listed

in Table 4. Most of the YSOs in these regions have no radial velocities in the Gaia DR2 catalog, thus we will use literature values of the radial velocities of YSOs or the gas in the clouds.

The central position of the star-forming regions will be expressed in a rectangular coordinate system  $(x, y, z)$  with the Sun at the origin. The  $(Ox)$ -axis is defined in the line of the Sun-Galactic center direction (the positive direction is towards the Galactic center). The  $(Oy)$ -axis is in the galactic plane and orthogonal to the  $(Ox)$ -axis (positive values in the direction of the galactic rotation). The  $(Oz)$ -axis is orthogonal to the Galactic plane with positive values towards the Galactic North pole. The coordinate system  $(Oxyz)$  is right handed. The positions  $(X, Y, Z)$  of the star-forming regions are listed in Table 5. The three-dimensional heliocentric velocities  $(U, V, W)$  of the star-forming regions in this reference frame are obtained directly from the mean proper motions and radial velocities of Table 4 and listed in Table 5. The  $(U, V, W)$  velocities are transformed to the Local Standard of Rest (LSR) velocities  $(u, v, w)$  by subtracting the motion of

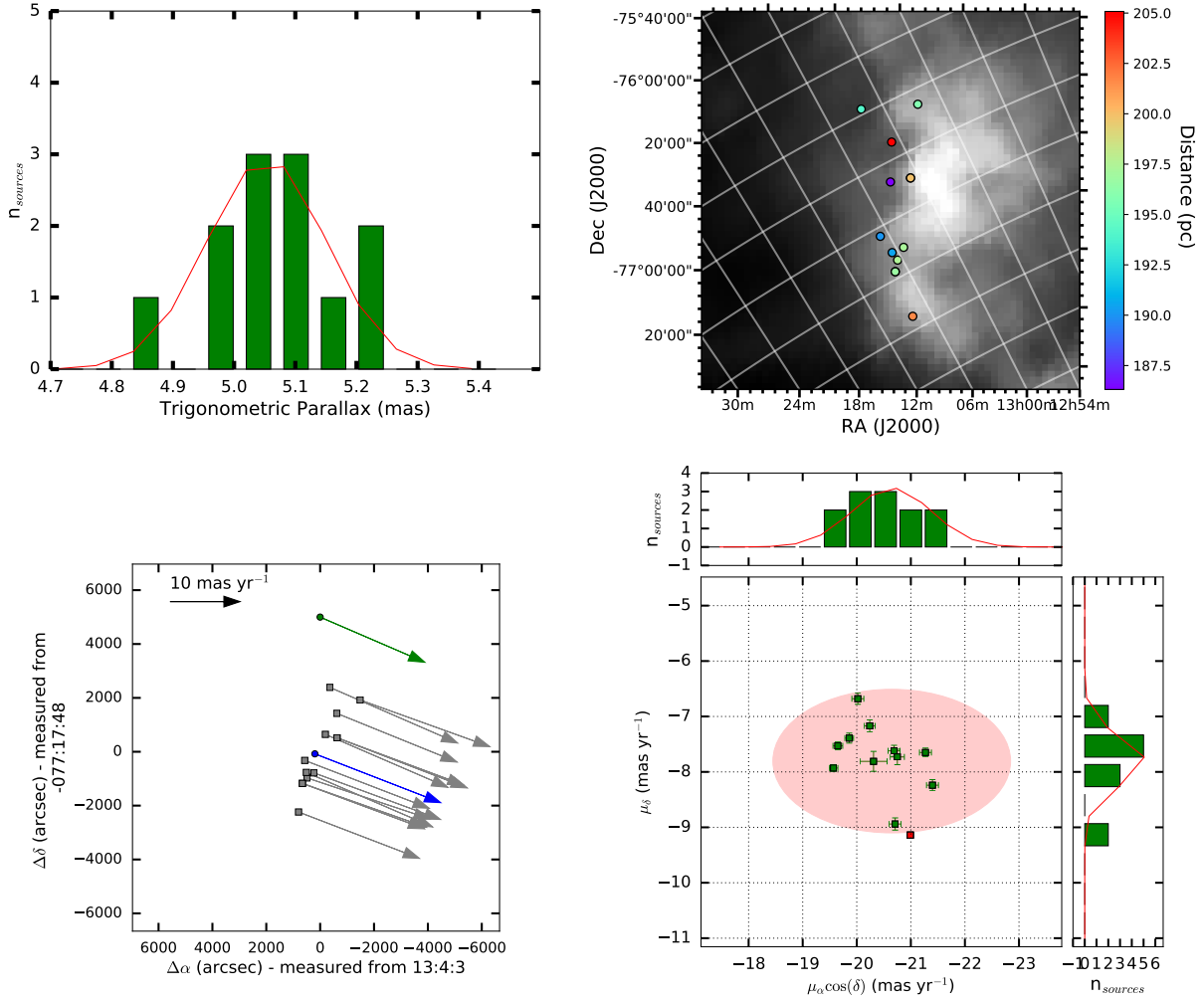


**Figure 5.** Same as Figure 1, but for Chamaeleon II.

the Sun relative to the LSR. This motion is  $(U_{\odot}, V_{\odot}, W_{\odot}) = (11.1 \pm 0.7, 12.2 \pm 0.47, 7.25 \pm 0.37)$  km s $^{-1}$  (Schönrich et al. 2010). We also assumed a distance to the Galactic center of 8.4 kpc (Reid et al. 2009). The  $(u, v, w)$  velocities of the stars forming regions are listed in Table 5 and plotted in Figures 13 and 14.

Now we use the  $(X, Y, Z)$  positions listed in Table 5 to fit an ellipsoid that approximates the spatial distribution of the regions. To fit the ellipsoid, we use a singular value decomposition approach and the minimum volume enclosing ellipsoid method (Moshtagh 2009). The resulting best-fit parameters for the geometric center of the ellipsoid are  $(X_0, Y_0, Z_0) = (-82 \pm 15, 39 \pm 7, -25 \pm 4)$  pc, while the resulting ellipsoid sizes are  $(358 \pm 7) \times (316 \pm 13) \times (70 \pm 4)$  pc. The inclination angle of the ellipsoid with respect to the Galactic plane is  $21^{\circ}4 \pm 0^{\circ}9$ , and the direction of the ascending node is at  $\ell = 319^{\circ}4 \pm 2^{\circ}3$ . These parameters are in good agreement with recent estimates of the Gould Belt properties based on samples of massive O–B stars, which trace a fairly flat system with semiaxes  $\sim 350 \times 250 \times 50$  pc (i.e. Bobylev

& Bajkova 2014) and center in the second Galactic quadrant. We note that the shape of our ellipsoid, however, is closer to an oblate spheroid than other previous results. Differences may come from the different studied objects and from the more accurate distances used for our analysis.

The velocity vectors ( $\mathbf{v}$ ) of the star forming regions can now be used to investigate ordered motions with respect to the central position of our fitted ellipsoid. The position of each region is given by a vector  $r_R$  in this reference system, and it has an associated unit vector  $\hat{r}_R = r_R / |r_R|$ . Rivera et al. (2015) argue that the mean value of the scalar products of the unit vector and the velocity vector may be used as a proxy to the values of expansion/contraction of a cluster. Following these authors, we now use the scalar products to measure the expansion velocity of the star-forming regions in the Gould Belt relative to the center of the fitted ellipsoid. Using the LSR velocities from Table 5 we estimated the mean of their scalar products to be  $\overline{\hat{r}_R \cdot v} = 2.5 \pm 0.1$  km s $^{-1}$ , and a dispersion of  $\sigma_{\hat{r}_R \cdot v} = 0.8$  km s $^{-1}$ . Our results indicate that the ordered

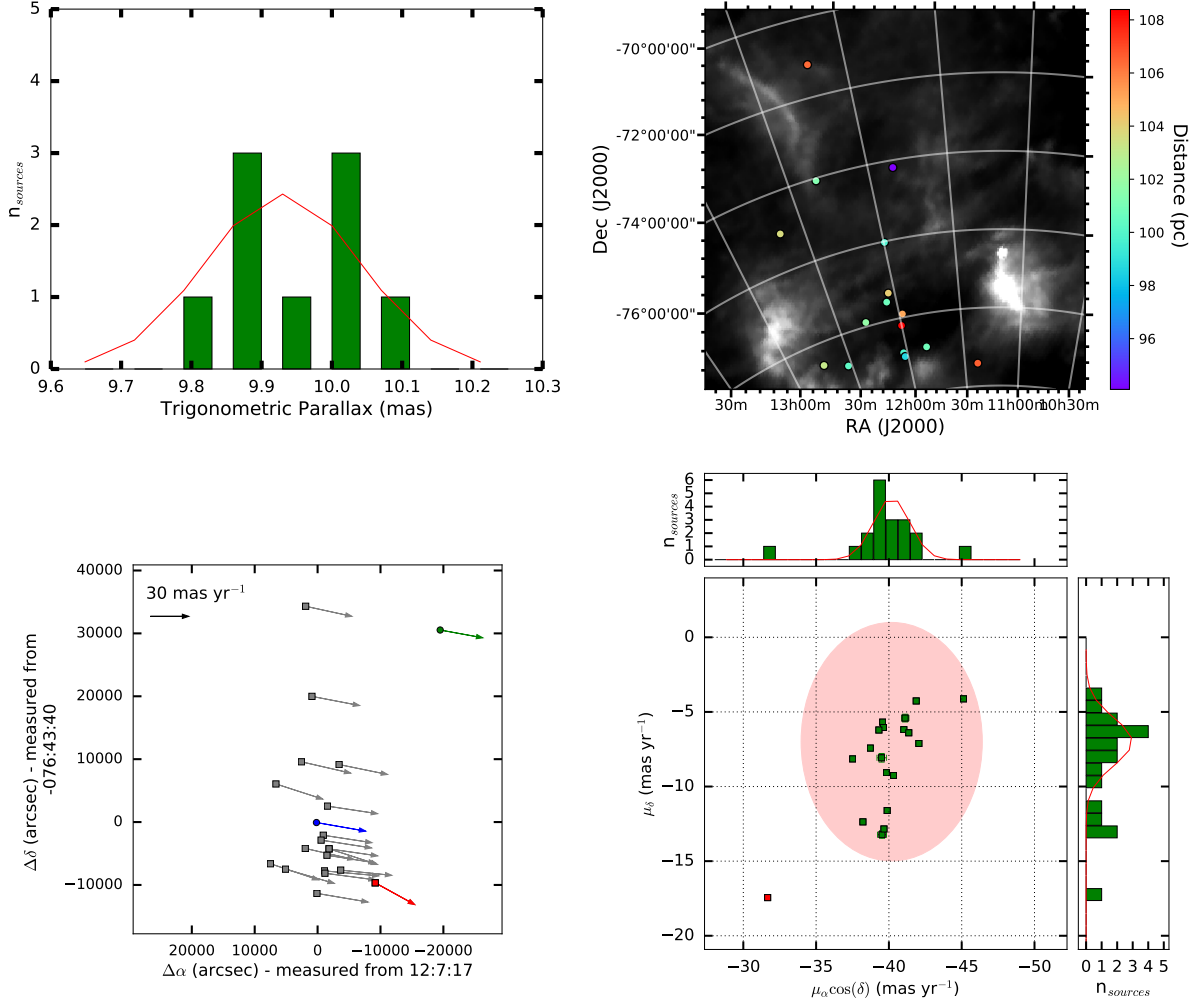


**Figure 6.** Same as Figure 1, but for  $\epsilon$  Chamaleontis. Red circle in the bottom right panel in this case is five times the proper motion dispersion measurement.

motion of the analyzed star-forming regions agrees with an expansion motion.

The initial expansion velocity of the GB is unknown. By assuming a simple free expansion model (i.e. the interaction of the GB with the interstellar medium (ISM) is negligible), Lindblad et al. (1973) estimated an initial expansion velocity of  $3.6 \text{ km s}^{-1}$ . By assuming that the GB-ISM interaction has decelerated the expansion, other authors have proposed even higher values, from 20 to  $60 \text{ km s}^{-1}$  (e.g., Olano 1982; Moreno et al. 1999). Even when considering the former case, our result indicates that the GB expansion has decreased. This effect may be caused by the GB-ISM interaction, or be due to distortion of the expansion by the Galactic gravitational potential (e.g., Perrot & Grenier 2003; Vasilkova 2014). The Galactic gravitational potential causes the elongation of the initial circular expansion, but it also affects the velocities of the components, with respect to the center of the expansion, as each component follows its own epicyclic orbit (see for example the model in Figure 9 from

Perrot & Grenier 2003). From Figure 13 we see that the velocity vectors of the studied regions are consistent with an average of  $10 \text{ km s}^{-1}$  (see also information on Table 3). The small dispersion value of  $\sigma_{\widehat{R} \cdot v} = 0.8 \text{ km s}^{-1}$ , points out to a small distortion of the expansion. Both the small distortion of the expansion and the near oblate spheroid shape obtained from our geometric fit, suggest that the age of the GB must be younger than previously thought or that the initial expansion velocity was high (see discussion by Moreno et al. 1999).

Recently, the existence of the GB has been proposed as a projection effect rather than a true ring of clouds (Bouy & Alves 2015). Our results, however, show that even when assuming that the star-forming regions in the GB are not part of a continuous ring, they seem to share the same kinematic expansion.

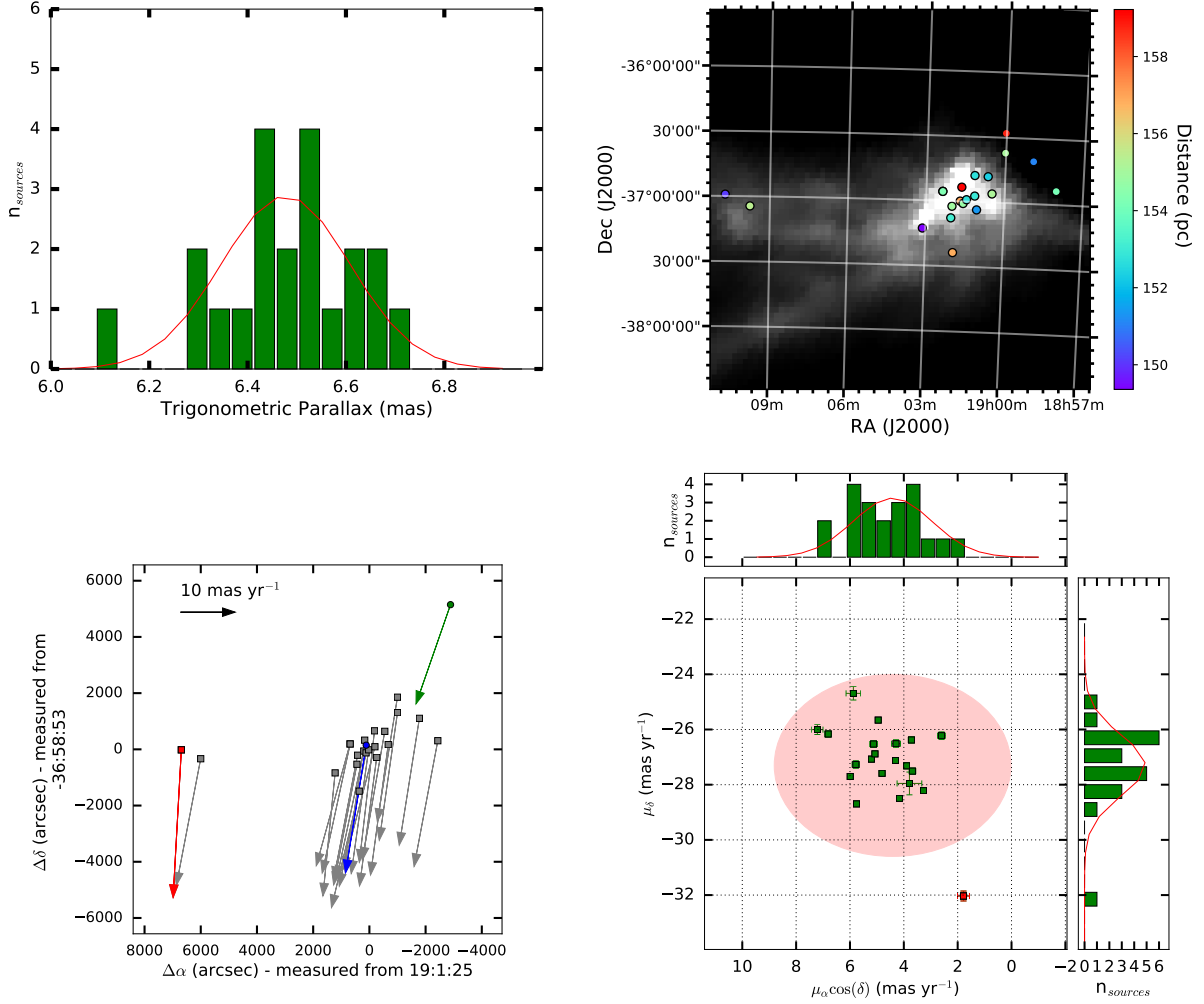


Figure 7. Same as Figure 1, but for Corona Australis

## 5. CONCLUSIONS

We have presented an analysis of YSOs in star-forming regions related to the Gould Belt that have an astrometric solution in the Gaia DR2 catalog. The estimated mean distances to each star-forming region are consistent with previous estimations. However, these new estimations have significant improvements to the final errors. The new distances were used to fit an ellipsoid to these regions, with the center located at  $(X_0, Y_0, Z_0) = (-82 \pm 15, 39 \pm 7, -25 \pm 4)$  pc, and dimensions of  $(358 \pm 7) \times (316 \pm 13) \times (70 \pm 4)$  pc, these values are consistent with those found for nearby O–B stars. We also obtained the mean proper motions of these star-forming regions that were combined with radial velocities from the literature to obtain their three-dimensional motion. The motion of the star-forming regions is consistent with them moving away from the center of the Gould Belt at a velocity of  $2.5 \text{ km s}^{-1}$ , in agreement with an expansion of the Gould Belt. This is the first time that YSOs motions are used to investigate the kinematics of the Gould Belt.

As an interesting side result of our analysis, we also identified stars with motions significantly larger than other stars in the same region. We speculated that some of them gained their peculiar motion via  $n$ -body interactions.

G.-N.O.L acknowledges support from the Alexander von Humboldt Foundation in the form of a Humboldt Fellowship. L.R. and L.L. acknowledges the financial support of DGAPA, UNAM (project IN112417), and CONACyT, México. This work has made use of data from the European Space Agency (ESA) mission *Gaia* (<https://www.cosmos.esa.int/gaia>), processed by the *Gaia* Data Processing and Analysis Consortium (DPAC, <https://www.cosmos.esa.int/web/gaia/dpac/consortium>). Funding for the DPAC has been provided by national institutions, in particular the institutions participating in the *Gaia* Multilateral Agreement. This research has made use of the SIMBAD database, operated at CDS, Strasbourg, France.

*Facilities:* Gaia

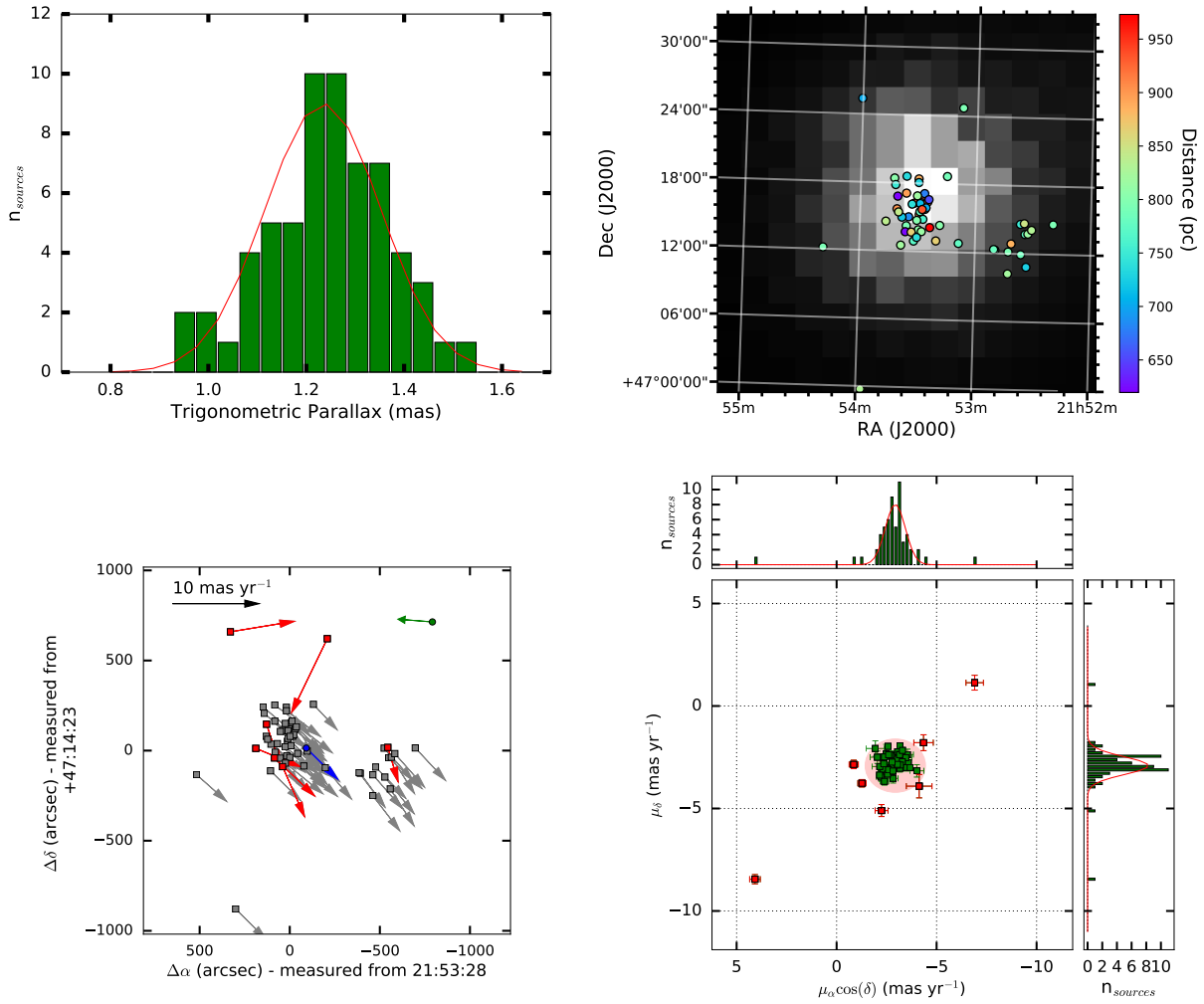


**Figure 8.** Same as Figure 1, but for IC 5146.

## REFERENCES

- Alves, F. O. & Franco, G. A. P. 2007, *A&A*, 470, 597
- Alves, J., Lombardi, M., & Lada, C. J. 2008, *The Pipe Nebula: A Young Molecular Cloud Complex*, ed. B. Reipurth, 415
- Bekki, K. 2009, *MNRAS*, 398, L36
- Biazzo, K., Alcalá, J. M., Covino, E., et al. 2012, *A&A*, 547, A104
- Bobylev, V. V. & Bajkova, A. T. 2014, *Astronomy Letters*, 40, 783
- Bouy, H. & Alves, J. 2015, *A&A*, 584, A26
- Brooke, T. Y., Huard, T. L., Bourke, T. L., et al. 2007, *ApJ*, 655, 364
- Comeron, F. 1993, *PASP*, 105, 441
- Comerón, F. 2008, *The Lupus Clouds*, ed. B. Reipurth, 295
- Crampton, D. & Fisher, W. A. 1974, *Publications of the Dominion Astrophysical Observatory Victoria*, 14, 283
- Crawford, I. A. 2000, *MNRAS*, 317, 996
- Dzib, S. A., Loinard, L., Rodríguez, L. F., et al. 2017, *ApJ*, 834, 139
- Dzib, S. A., Ortiz-León, G. N., Loinard, L., et al. 2018, *ApJ*, 853, 99
- Dzib, S. A., Ortiz-León, G. N., Loinard, L., et al. 2016, *ApJ*, 826, 201
- Elias, J. H. 1978, *ApJ*, 223, 859
- Feigelson, E. D., Lawson, W. A., & Garmire, G. P. 2003, *ApJ*, 599, 1207
- Franco, G. A. P. 1990, *A&A*, 227, 499
- Friesen, R. K., Pineda, J. E., co-PIs, et al. 2017, *ApJ*, 843, 63
- Gaia Collaboration, Brown, A. G. A., Vallenari, A., et al. 2018, *ArXiv e-prints* [1804.09365]
- Gaia Collaboration, Prusti, T., de Bruijne, J. H. J., et al. 2016, *A&A*, 595, A1
- Galli, P. A. B., Bertout, C., Teixeira, R., & Ducourant, C. 2013, *A&A*, 558, A77
- Galli, P. A. B., Loinard, L., Ortiz-León, G. N., et al. 2018, *ApJ*, 859, 33

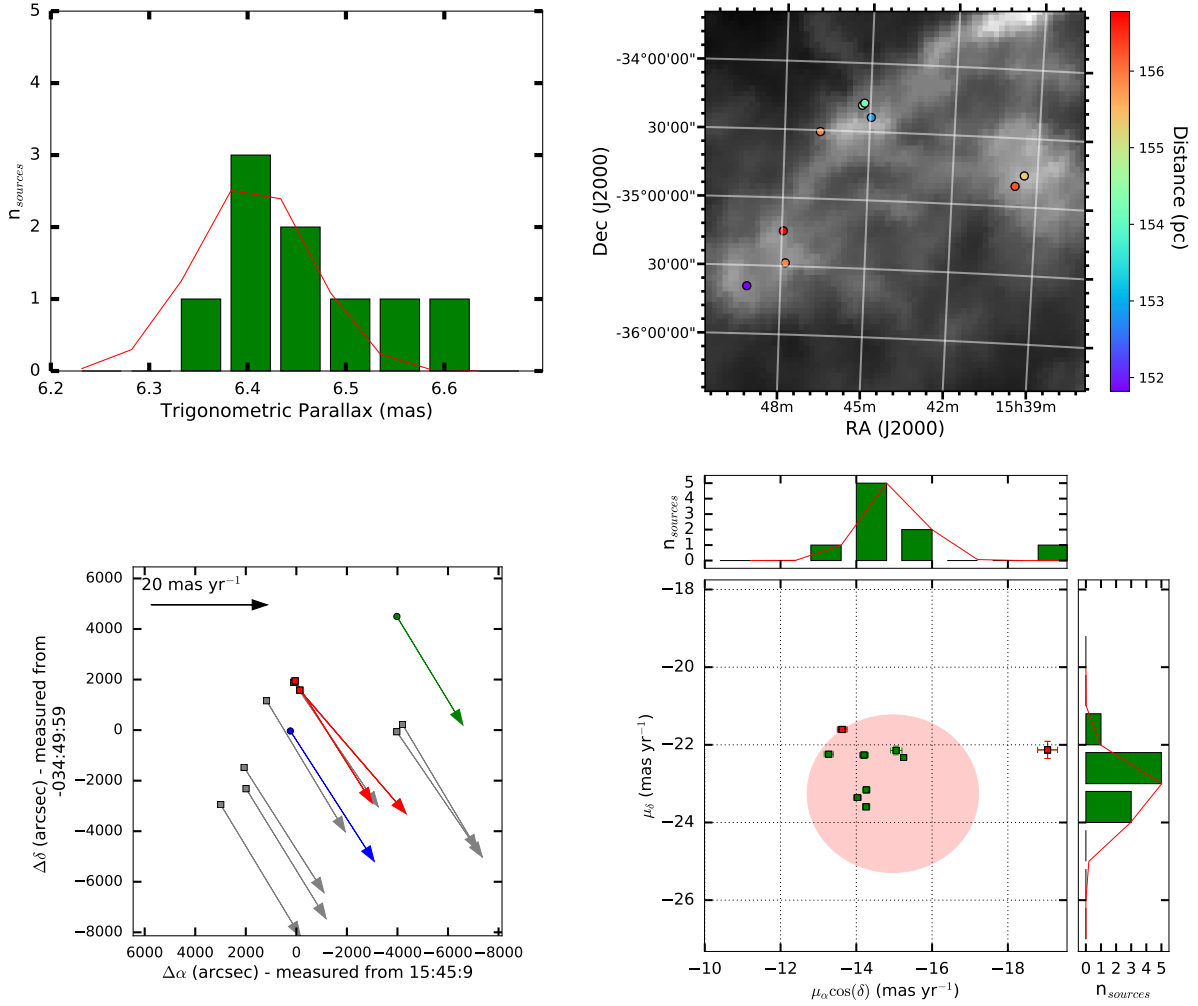


**Figure 9.** Same as Figure 1, but for Lupus 1.

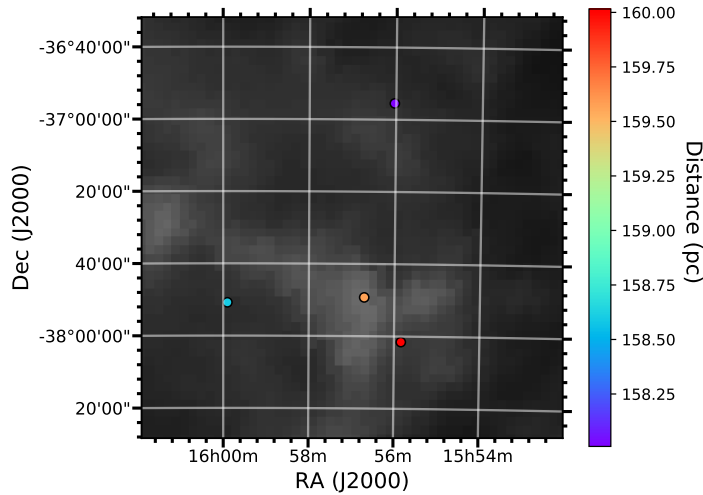


**Figure 10.** Spatial distribution of YSOs in Lupus 2 that appear in the Gaia DR2 catalog.

- García-Díaz, M. T., Henney, W. J., López, J. A., & Doi, T. 2008, *RMxAA*, 44, 181
- Guillout, P., Sterzik, M. F., Schmitt, J. H. M. M., Motch, C., & Neuhaeuser, R. 1998, *A&A*, 337, 113
- Herbig, G. H. & Reipurth, B. 2008, *Young Stars and Molecular Clouds in the IC 5146 Region*, ed. B. Reipurth, 108
- Hu, E. M. 1981, *ApJ*, 248, 119
- Joergens, V. 2006, *A&A*, 448, 655
- Kounkel, M., Hartmann, L., Loinard, L., et al. 2017, *ApJ*, 834, 142
- Kun, M., Kiss, Z. T., & Balog, Z. 2008, *Star Forming Regions in Cepheus*, ed. B. Reipurth, 136
- Lada, C. J., Alves, J., & Lada, E. A. 1999, *ApJ*, 512, 250
- Lada, C. J., Lada, E. A., Clemens, D. P., & Bally, J. 1994, *ApJ*, 429, 694
- Lebrun, F. 1986, *ApJ*, 306, 16
- Lindblad, P. O., Grape, K., Sandqvist, A., & Schober, J. 1973, *A&A*, 24, 309
- Lombardi, M., Alves, J., & Lada, C. J. 2006, *A&A*, 454, 781
- Lombardi, M., Lada, C. J., & Alves, J. 2008, *A&A*, 489, 143

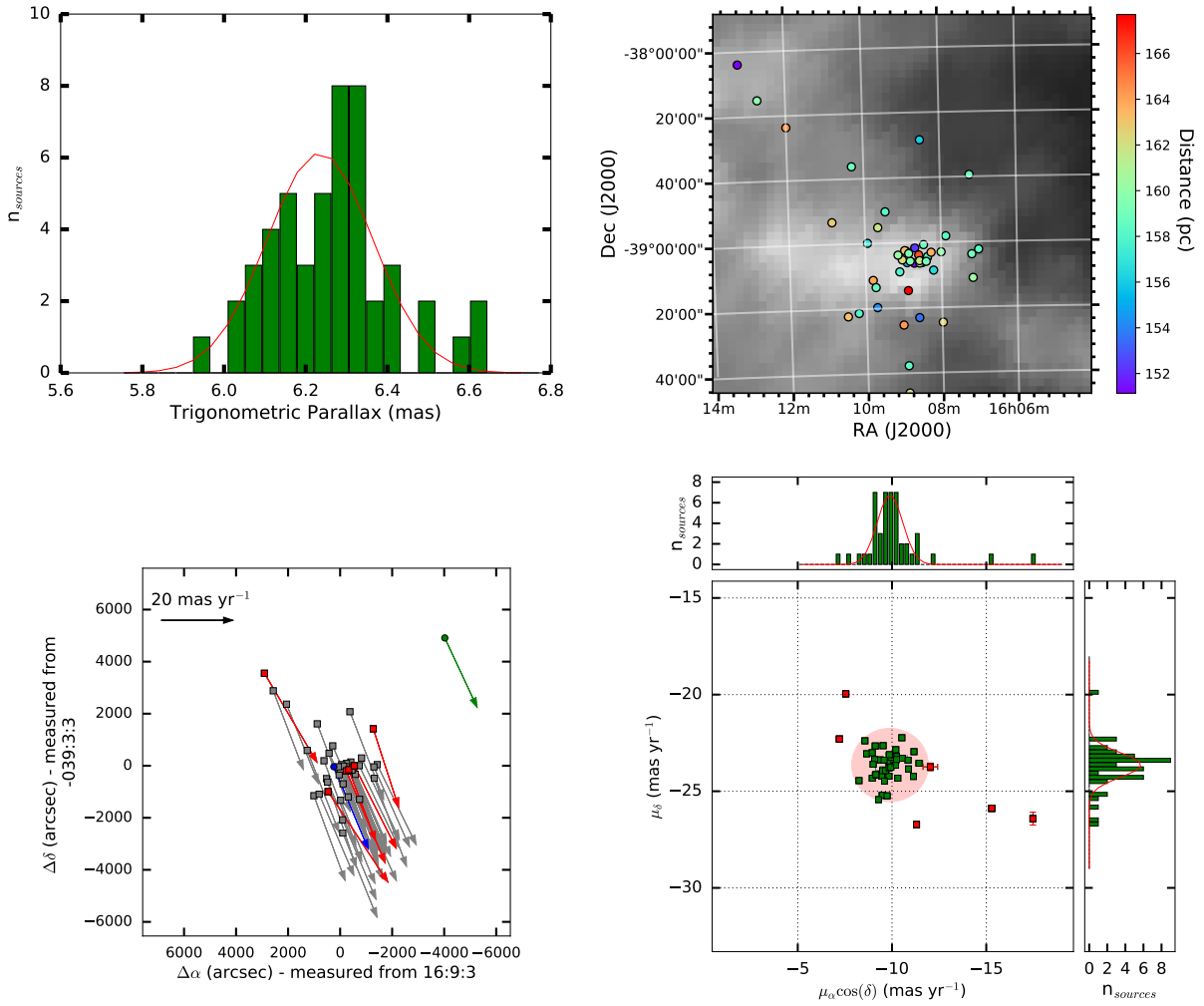


**Figure 11.** Same as Figure 1, but for Lupus 3.

- Luhman, K. L. 2004, *ApJ*, 616, 1033
- Luhman, K. L. 2008, *Chamaeleon*, ed. B. Reipurth, 169
- Luri, X., Brown, A. G. A., Sarro, L. M., et al. 2018, *ArXiv e-prints* [1804.09376]
- Moreno, E., Alfaro, E. J., & Franco, J. 1999, *ApJ*, 522, 276
- Moshtagh, N. 2009, *MINIMUM VOLUME ENCLOSING ELLIPSOIDS*
- Neuhäuser, R. & Forbrich, J. 2008, *The Corona Australis Star Forming Region*, ed. B. Reipurth, 735
- Neuhäuser, R., Walter, F. M., Covino, E., et al. 2000, *A&AS*, 146, 323
- Olano, C. A. 1982, *A&A*, 112, 195
- Olano, C. A., Meschin, P. I., & Niemela, V. S. 2006, *MNRAS*, 369, 867
- Ortiz-León, G. N., Dzib, S. A., Kounkel, M. A., et al. 2017a, *ApJ*, 834, 143
- Ortiz-León, G. N., Loinard, L., Dzib, S. A., et al. 2018, *ArXiv e-prints* [1808.03499]
- Ortiz-León, G. N., Loinard, L., Kounkel, M. A., et al. 2017b, *ApJ*, 834, 141
- Perrot, C. A. & Grenier, I. A. 2003, *A&A*, 404, 519
- Poveda, A., Ruiz, J., & Allen, C. 1967, *Boletín de los Observatorios Tonantzintla y Tacubaya*, 4, 86
- Racine, R. 1968, *AJ*, 73, 233
- Redaelli, E., Alves, F. O., Caselli, P., et al. 2017, *ApJ*, 850, 202
- Reid, M. J., Menten, K. M., Zheng, X. W., et al. 2009, *ApJ*, 700, 137
- Reipurth, B. & Zinnecker, H. 1993, *A&A*, 278, 81
- Rivera, J. L., Loinard, L., Dzib, S. A., et al. 2015, *ApJ*, 807, 119
- Schönrich, R., Binney, J., & Dehnen, W. 2010, *MNRAS*, 403, 1829
- Straizys, V., Maskoliūnas, M., Boyle, R. P., et al. 2014, *MNRAS*, 438, 1848
- Vasilkova, O. O. 2014, *Astronomy Letters*, 40, 59
- Voirin, J., Manara, C. F., & Prusti, T. 2018, *A&A*, 610, A64
- Ward-Thompson, D., Di Francesco, J., Hatchell, J., et al. 2007, *PASP*, 119, 855

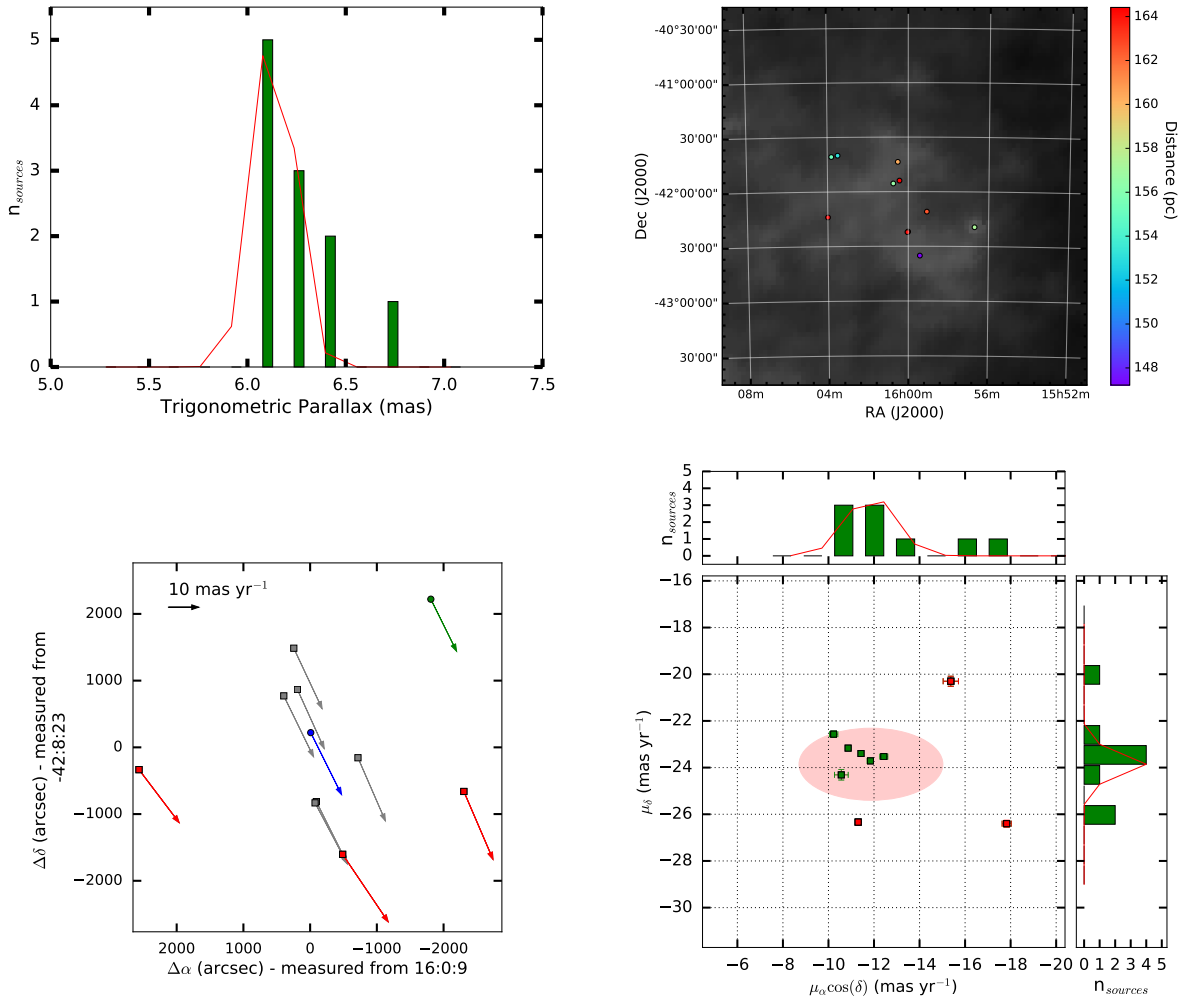


Figure 12. Same as Figure 1, but for Lupus 4.

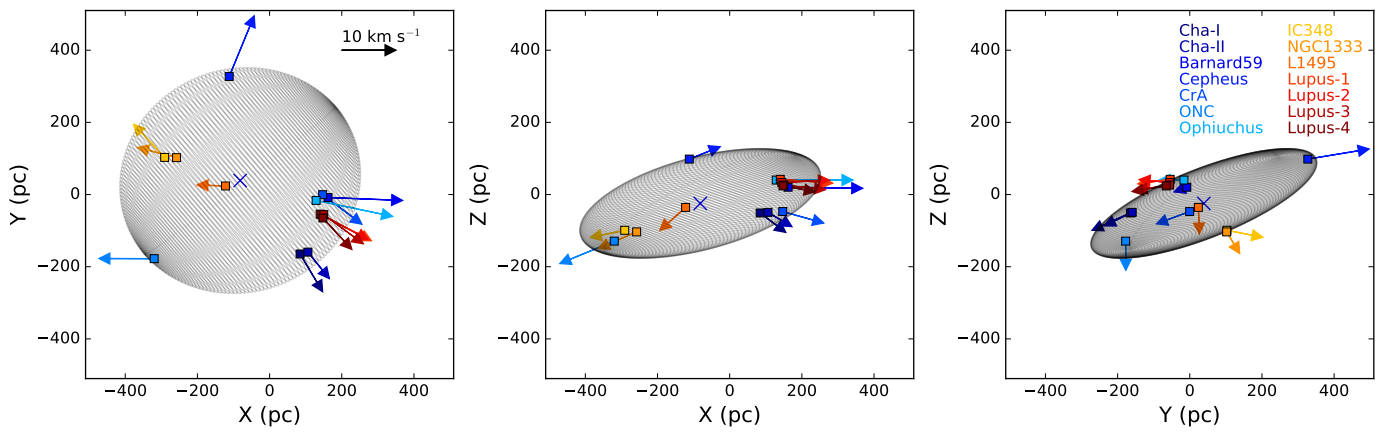


Figure 13. Motion of the star-forming region in the Gould Belt in the three planes: X-Y (left), X-Z (center), and Y-Z (right). The projection of the fitted ellipsoid is also plotted.



**Table 4.** Distances, mean proper motions, and mean radial velocities of star-forming regions in the Gould Belt.

Region	D (pc)	$\mu_{\alpha*}$ (mas yr <sup>-1</sup> )	$\mu_{\delta}$ (mas yr <sup>-1</sup> )	RV (km s <sup>-1</sup> )	References
Barnard 59	163 ± 5	-1.2 ± 0.2	-19.2 ± 0.1	3.4 ± 0.11	1,2
Cepheus Flare	360 ± 32	6.0 ± 0.2	0.4 ± 0.5	0.0	1,3
Chamaeleon I	192 ± 6	-22.8 ± 0.1	0.3 ± 0.1	14.7 ± 1.3	1,4
Chamaeleon II	198 ± 6	-20.7 ± 0.1	-8.0 ± 0.1	11.4 ± 2.0	1,5
Corona Australis	154 ± 4	4.4 ± 0.2	-27.3 ± 0.2	-1.0 ± 1.0	1,6
Lupus 1	156 ± 3	-15.0 ± 0.1	-23.3 ± 0.1	2.5 ± 1.6	1,7
Lupus 2	159 ± 3	-10.7 ± 0.1	-22.0 ± 0.1	2.2 ± 0.9	1,7
Lupus 3	162 ± 3	-10.0 ± 0.1	-23.7 ± 0.1	1.0 ± 0.7	1,7
Lupus 4	163 ± 4	-11.9 ± 0.2	-23.9 ± 0.2	0.3 ± 3.8	1,7
ONC	388 ± 5	-1.1 ± 0.1	-0.8 ± 0.2	27 ± 2	8,9,10
L 1688 (Ophiuchus)	137 ± 1	-5.28 ± 0.02	-26.06 ± 0.08	3.6	11,12
IC 348 (Perseus)	321 ± 10	4.34 ± 0.03	-6.76 ± 0.01	15.9 ± 1.8	13
NGC 1333 (Perseus)	293 ± 22	7.34 ± 0.05	-9.90 ± 0.03	14.8 ± 1.3	13
L 1495 (Taurus)	129.5 ± 0.3	8.56 ± 0.10	-25.3 ± 0.1	15.1 ± 0.6	14

**References**—1=This work, 2=Redaelli et al. (2017), 3=Kun et al. (2008), 4=Joergens (2006), 5=Biazzo et al. (2012), 6=Neuhäuser et al. (2000), 7=Galli et al. (2013), 8=Kounkel et al. (2017), 9=Dzib et al. (2017), 10=García-Díaz et al. (2008), 11=Ortiz-León et al. (2017b), 12=Friesen et al. (2017), 13=Ortiz-León et al. (2018), and 14=Galli et al. (2018).

**Table 5.** Heliocentric and LSR velocities, and heliocentric positions of star-forming regions in the Gould Belt.

Region	$U$ (km s <sup>-1</sup> )	$V$ (km s <sup>-1</sup> )	$W$ (km s <sup>-1</sup> )	$u$ (km s <sup>-1</sup> )	$v$ (km s <sup>-1</sup> )	$w$ (km s <sup>-1</sup> )	X (pc)	Y (pc)	Z (pc)
Barnard 59	3.6 ± 1.0	-12.8 ± 0.1	-7.5 ± 0.2	14.7 ± 1.2	-0.6 ± 0.5	-0.2 ± 0.4	161.9 ± 5.0	-8.3 ± 0.3	20.3 ± 0.6
Cepheus	-6.3 ± 3.8	-0.6 ± 2.4	-5.3 ± 3.4	4.8 ± 3.9	11.7 ± 2.4	1.9 ± 3.4	-111.9 ± 10.0	327.1 ± 29.3	98.2 ± 8.8
Cha I	-7.2 ± 0.9	-18.8 ± 0.9	-10.2 ± 1.1	3.9 ± 1.1	-6.6 ± 1.0	-3.0 ± 1.1	84.4 ± 2.6	-164.7 ± 5.1	-51.0 ± 1.6
Cha II	-7.7 ± 1.2	-16.4 ± 1.6	-9.3 ± 0.6	3.4 ± 1.4	-4.2 ± 1.7	-2.0 ± 0.7	106.2 ± 2.7	-159.5 ± 4.1	-49.4 ± 1.3
CrA	-4.0 ± 1.0	-17.6 ± 0.8	-9.2 ± 1.0	7.1 ± 1.2	-5.3 ± 0.9	-2.0 ± 1.1	147.0 ± 3.9	-0.3 ± 0.1	-47.1 ± 1.2
Lupus 1	-1.5 ± 1.5	-17.2 ± 0.8	-7.9 ± 0.7	9.6 ± 1.6	-5.0 ± 0.9	-0.7 ± 0.8	140.2 ± 2.7	-54.3 ± 1.0	42.2 ± 0.8
Lupus 2	-2.6 ± 0.9	-16.8 ± 0.7	-6.8 ± 0.6	8.5 ± 1.1	-4.6 ± 0.8	0.4 ± 0.7	144.5 ± 2.8	-55.7 ± 1.1	33.2 ± 0.6
Lupus 3	-4.0 ± 0.7	-17.5 ± 0.6	-8.0 ± 0.5	7.1 ± 1.0	-5.2 ± 0.7	-0.8 ± 0.6	150.2 ± 3.9	-55.8 ± 1.4	26.4 ± 0.7
Lupus 4	-6.1 ± 3.4	-17.7 ± 1.5	-8.1 ± 0.6	5.0 ± 3.5	-5.4 ± 1.6	-0.9 ± 0.7	147.7 ± 3.4	-65.0 ± 1.5	24.0 ± 0.5
ONC	-21.3 ± 1.7	-12.2 ± 1.0	-11.5 ± 0.7	-10.2 ± 1.8	0.0 ± 1.1	-4.2 ± 0.8	-319.9 ± 4.4	-177.7 ± 2.4	-129.1 ± 1.8
Ophiuchus	4.1 ± 0.9	-15.6 ± 0.1	-7.3 ± 0.3	15.2 ± 1.2	-3.3 ± 0.5	-0.1 ± 0.5	130.2 ± 1.1	-16.3 ± 0.1	40.5 ± 0.3
IC348	-17.0 ± 1.6	-6.1 ± 0.6	-8.5 ± 0.6	-5.9 ± 1.8	6.1 ± 0.7	-1.3 ± 0.7	-287.7 ± 9.2	101.8 ± 3.2	-98.0 ± 3.1
NGC1333	-17.3 ± 1.2	-10.7 ± 0.5	-9.9 ± 0.5	-6.2 ± 1.3	1.6 ± 0.7	-2.7 ± 0.6	-257.8 ± 19.7	102.3 ± 7.8	-103.5 ± 7.9
L 1495	-15.2 ± 0.6	-12.1 ± 0.1	-10.9 ± 0.2	-4.1 ± 0.9	0.1 ± 0.5	-3.6 ± 0.4	-122.2 ± 0.3	23.8 ± 0.1	-35.7 ± 0.1

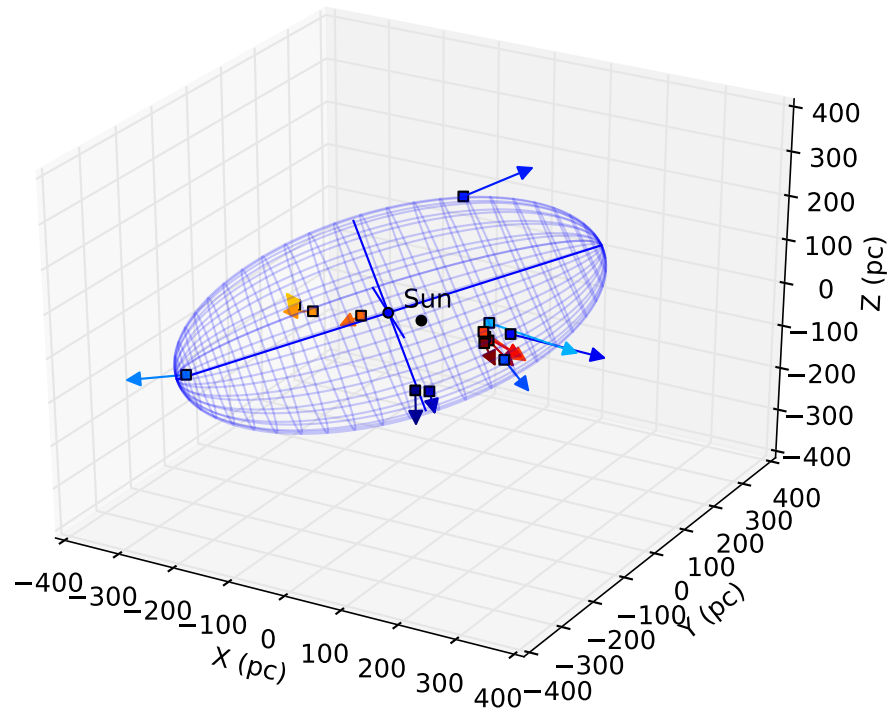


**Figure 14.** Three dimensional motion of star-forming regions in the Gould Belt (colored arrows same as in figure 13). Position of the Sun and the Center of the Gould Belt (GBC) are indicated as black and blue circles, respectively. Fitted ellipsoid is also plotted.